QNTN: Establishing a Regional Quantum Network in Tennessee

Mohamed Shaban[§,†], Muhammad Ismail[§], and Mariam Kiran[‡]
[§]Cybersecurity Education, Research, and Outreach Center (CEROC) and Computer Science Department, Tennessee Tech University, TN, USA
[†]Department of Mathematics, Faculty of Education, Alexandria University, Egypt
[‡]Oak Ridge National Laboratory, TN, USA
Emails: {mmibrahims42, mismail}@tntech.edu, kiranm@ornl.gov

***Abstract*—This paper investigates the design of a regional Quantum Network in Tennessee (QNTN) that will connect three quantum local area networks in different cities. We explore two approaches for achieving this interconnection: deploying a satellite constellation in the space layer and employing high-altitude platforms (HAPs) in the aerial layer. Our comparison reveals that a space-ground architecture that uses 108 satellites provides 55.17% coverage of the day and handles 57.75% of entanglement distribution requests with an average fidelity of 0.96. In contrast, the air-ground architecture delivers full-day coverage, fulfills 100% of requests, and achieves a higher average fidelity of 0.98. However, HAPs face significant challenges such as limited operational time, sensitivity to vibrations and weather conditions, and the need for continuous maintenance. This paper contributes to the understanding of optimal architecture for regional quantum networks, highlighting the trade-offs between satellite-based and air-ground approaches.**

***Index Terms*—Quantum Internet, regional quantum networks, quantum communications, entanglement distribution, entanglement fidelity, satellites, high-altitude platforms.**

I. Introduction

The Quantum Internet can revolutionize the security and speed of communications [1]–[4]. It also has the potential to enable applications such as secure delegated computing [5] and distributed quantum computing and sensing [6], [7]. Quantum entanglement is fundamental to connect nodes over quantum networks, as most applications depend on it. Thus, efficiently sharing entanglement among distant nodes is essential for enabling quantum Internet applications. As local quantum networks advance and become more widely deployed, exploring efficient strategies for linking local networks to achieve larger connectivity is vital. However, connecting distant quantum networks presents a significant challenge due to photon loss in fiber optic channels, which becomes substantial after a few tens of kilometers and hinders practical applications. Although vacuum beam guide (VBG) [8] technology is promising, it remains in its early stages and faces significant challenges. Photons naturally spread out in a vacuum, making it difficult to maintain a focused beam [9]. Moreover, creating and sustaining a high vacuum environment requires advanced systems and precise sealing techniques, where any leaks or contamination can severely impact beam quality. At the same time, free space optical (FSO) communication excels in communications over long distances, as optical loss scales quadratically with distance in FSO communication, in contrast to the exponential loss encountered in fiber optics. Several projects aim to establish quantum networks through FSO communications, such as China's Micius satellite [10] and EuroQCI [11]. Another way is to integrate the space layer as a promising approach, but it poses challenges such as interrupted services due to the absence of satellites at certain times, dictated by their orbital trajectories.

To realize the quantum Internet, this paper explores an architectural design for a regional Quantum Network in Tennessee (QNTN) that connects local quantum networks at Tennessee Tech University, Oak Ridge National Laboratory, and the EBP commercial network. To achieve this goal, we investigate two approaches for interconnection: a satellite constellation in the space layer and high altitude platforms (HAPs) in the aerial layer. We evaluate each approach in terms of coverage period, entanglement fidelity, and percentage of served requests to determine their feasibility and effectiveness.

A. Related Work

Existing implementations of quantum networks primarily focus on local networks using fiber optic communication. For instance, the work in [12] constructed a first-generation commercial quantum network with all nodes placed in a single building. The work in [13] designed the Boston-area quantum network, connecting three different institutions: MIT Lincoln Laboratory (MITLL), MIT, and Harvard University, with the longest quantum channel between MIT and MITLL measuring 42.5 km.

Efforts targeting regional coverage are yet to be deployed. The work in [14] investigates a quantum network connecting transmitters in Trieste (Italy) and Ljubljana (Slovenia) with receivers in Postojna (Slovenia) and Rijeka (Croatia) for quantum key distribution (QKD) services. This network relies on fiber optic channels and uses trusted nodes to measure and re-encode quantum states, extending the transmission distance of the quantum states. The work in [15] investigates using satellites and high-altitude balloons to connect two quantum cities in Europe, Paris and Delft, separated by 377 km. Additionally, the EuroQCI project [11] is working to establish

This work was supported by NSF Award # 2210251.

quantum networks using satellites, aiming to extend quantum communication capabilities. Although China's Micius [10] is an operational satellite, it currently serves only as a single satellite providing QKD between two nodes.

However, existing quantum network implementations [12], [13] are limited to local networks, where connected nodes are within a single building or separated by a limited distance. These implementations rely solely on fiber optic communication, which suffers from significant limitations when connecting networks or nodes over long distances. Regional networks that use fiber optic channels [14] are limited to QKD services and cannot support entanglement distribution, as they require measuring and re-encoding quantum states. Projects like EuroQCI and Micius demonstrate the potential of using space for connecting quantum nodes. The work in [15] also explores the use of satellites and HAPs for quantum network connections. Despite these efforts, they primarily focus on QKD services and do not address broader quantum communications. Moreover, there is a lack of analysis comparing air-ground architecture with space-ground architecture in terms of coverage period, served requests, and entanglement fidelity. This analysis is crucial for determining the optimal architecture to enable a wide range of applications.

B. Paper Contributions

We investigate two approaches to establish a regional quantum network that connects local area networks separated by large distances. This will help determine the best approach for building the QNTN network and pave the way for other networks to be built based on our analysis. Toward this overarching goal, we carry out the following contributions:

- We explore two architectures for connecting distant local quantum networks: a space-ground architecture utilizing a constellation of satellites and an air-ground architecture employing HAPs.
- We adopt the Bellman-Ford algorithm for entanglement routing within both architectures. This algorithm is used to distribute entanglement across the regional network and measure the achievable entanglement fidelity for each approach.
- We upgrade an existing quantum network simulator to simulate the proposed architectures and provide a performance evaluation. We use this upgraded version to conduct a comprehensive analysis of each approach, detailing the coverage period, entanglement fidelity of distributed pairs, and the percentage of served requests. Additionally, we provide a comparative analysis to highlight the effectiveness of each approach. Our findings show that the space-ground architecture, utilizing 108 satellites, offers 55.17% coverage throughout the day and handles 57.75% of entanglement distribution requests, with an average fidelity of 0.96. In contrast, the air-ground architecture achieves full-day coverage, serves 100% of requests, and achieves a higher average fidelity of 0.98. While the air-ground approach demonstrates superior performance, it is important to note that it faces significant challenges. These include limited operational time due to power constraints and susceptibility to environmental factors that affect signal transmission and platform stability. These challenges warrant further investigations for effective applicability in the near term.

TABLE I
COORDINATES OF GROUND NODES.

Tennessee Tech University		
(36.1757,−85.5066)	(36.1751,−85.5067)	(36.1754,−85.5074)
(36.1755,−85.5058)	(36.1756,−85.5080)	
EBP commercial network		
(35.04159,−85.2799)	(35.04169,−85.2801)	(35.04179,−85.2803)
(35.04189,−85.2805)	(35.04199,−85.2807)	(35.04051,−85.2806)
(35.04061,−85.2807)	(35.04071,−85.2808)	(35.04081,−85.2809)
(35.04091,−85.2810)	(35.03971,−85.2810)	(35.03981,−85.2811)
(35.03991,−85.2812)	(35.04001,−85.2813)	(35.04011,−85.2814)
Oak Ridge National Laboratory		
(35.91,−84.3)	(35.91,−84.303)	(35.918,−84.304)
(35.92,−84.321)	(35.927,−84.313)	(35.92380,−84.316)
(35.9285,−84.31283)	(35.9294,−84.3101)	(35.9293,−84.3106)
(35.9298,−84.3106)	(35.9309,−84.308)	

The rest of this paper is organized as follows. Section II presents the network architecture, detailing the local ground networks and the two approaches for connecting them: space-ground and air-ground architectures. Section III describes the channel models, details an entanglement routing algorithm based on Bellman-Ford, and discusses our upgrades to an existing quantum network simulator for performance evaluation. Section IV provides simulation results and compares the performance metrics of the space-ground and air-ground approaches. Section V concludes the paper and discusses future research directions.

II. NETWORK ARCHITECTURE

In this section, we provide a detailed description of the local networks involved in the QNTN, including the specific locations of each node. We then explore two architectures for connecting these local networks and establishing the QNTN regional network: the space-ground architecture using a satellite constellation and the air-ground architecture utilizing an HAP. Finally, we discuss the advantages and disadvantages of each architecture.

A. Ground Local Networks

The QNTN comprises three local networks, each consisting of multiple nodes interconnected via fiber optic channels. The first network, located at Tennessee Tech University, includes 5 nodes and covers the engineering quad. The second network, located at Oak Ridge National Laboratory, comprises 11 quantum nodes. The third network, the EPB commercial quantum network located at Chattanooga, includes 15 nodes. The three local networks are shown in Fig. 1. The coordinates of the ground nodes are detailed in Table I.

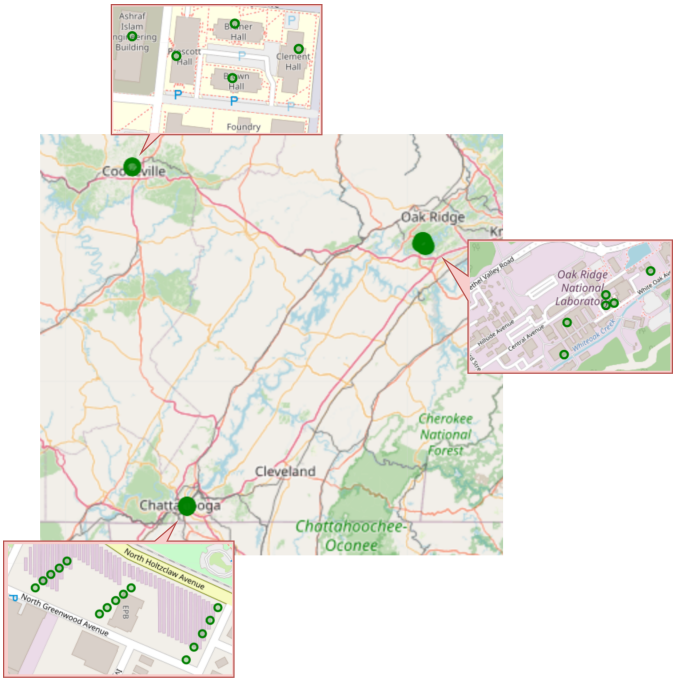

Fig. 1. Illustration of the three local networks in the QNTN on the map: Tennessee Tech University, Oak Ridge National Laboratory, and the EPB commercial quantum network.

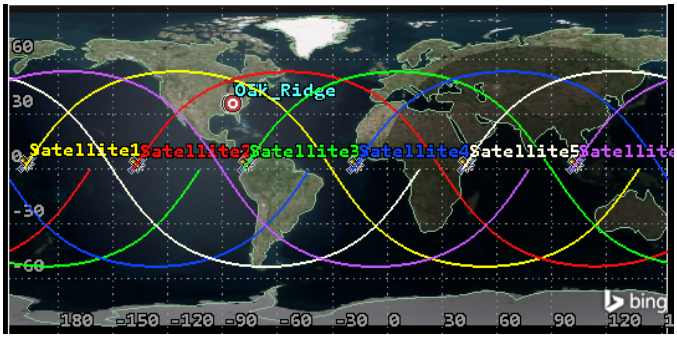

Fig. 2. Configuration of 6 orbital planes in the Walker Delta constellation, each plane spaced by 60 degrees in the RAAN.

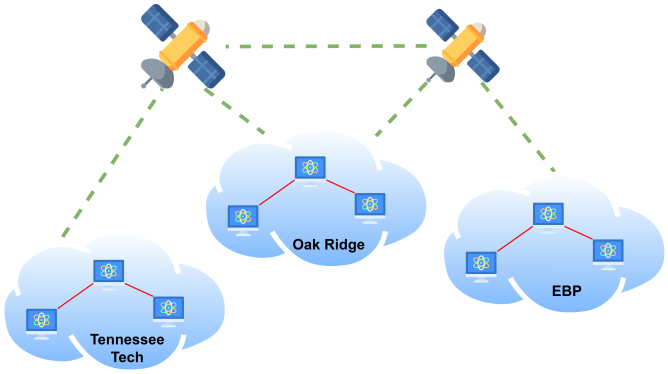

Fig. 3. Illustration of the space-ground architecture employing a satellite constellation to connect three local networks in Tennessee. Fiber optic channels are presented in red solid lines, while FSO channels are shown in green dashed lines.

To connect these three networks, we explore two different approaches. The first approach employs a space-ground architecture, while the second utilizes an air-ground architecture. This paper aims to evaluate each approach comprehensively and determine the most effective method for linking these three networks.

B. Space-Ground Architecture for Regional Network

In this architecture, satellites are employed to link the three local networks. In this paper, we experiment with varying numbers of satellites to evaluate the duration for which all three networks remain connected. We explore different configurations of a low Earth orbit (LEO) constellation to optimize coverage. LEO is chosen for its benefits in reducing latency and minimizing signal loss compared to higher orbits. Satellites are positioned at an altitude of 500 km, striking a balance between signal loss and operational lifespan.

We tested configurations with 6 to 108 satellites. For the first 36 satellites, we use a Walker Delta constellation configuration. This setup includes 6 orbital planes inclined at 53 degrees. Each plane is spaced 60 degrees apart in the right ascension of the ascending node (RAAN) with values of 0, 60, 120, 180, 240, and 300 degrees, as shown in Fig. 2. Each plane consists of 6 satellites positioned at true anomalies of 0, 60, 120, 180, 240, and 300 degrees. To further enhance coverage, we incrementally increase the number of satellites by filling the gaps between these orbital planes. Specifically, we add 12 additional orbital planes, ensuring that all planes are spaced 20 degrees apart in the RAAN. Each new plane also contains 6 satellites, positioned at true anomalies of 0, 60, 120, 180, 240, and 300 degrees. The semi-major axis for the satellite orbits is set to 6871 km, corresponding to an altitude of 500 km. The used satellite orbits are shown in Table II. The space-ground architecture is shown in Fig. 3.

C. Air-Ground Architecture for Regional Network

In this architecture, aerial vehicles are utilized to connect the three local networks. These vehicles can be unmanned aerial vehicles (UAVs) or HAPs. UAVs excel in flexibility and mobility, whereas HAPs offer superior long-endurance capabilities and wide-area coverage. The choice depends on trade-offs in endurance, payload capacity, altitude, and deployment complexity. In this work, we employ a single HAP to connect the three networks. The coordinates of the HAP are $(35.6692, -85.0662)$, and its altitude is 30 km. The air-ground architecture is shown in Fig. 4.

D. Discussion

In comparing space-ground and air-ground architectures for quantum communication networks, several key differences emerge. The space-ground approach, utilizing satellite constellations, offers wide coverage and high-altitude operation, which reduces atmospheric interference and enables global communication. However, it comes with significant challenges such as high latency due to the large distance between ground stations and satellites, high deployment costs, and limited maneuverability once satellites are in orbit. Conversely, the

TABLE II
SATELLITES ORBITAL CONFIGURATIONS.

Satellites					
RAAN (deg)	True Anomaly (deg)	RAAN (deg)	True Anomaly (deg)	RAAN (deg)	True Anomaly (deg)
0	0	20	0	200	0
60	0	20	60	200	60
120	0	20	120	200	120
180	0	20	180	200	180
240	0	20	240	200	240
300	0	20	300	200	300
0	60	40	0	220	0
60	60	40	60	220	60
120	60	40	120	220	120
180	60	40	180	220	180
240	60	40	240	220	240
300	60	40	300	220	300
0	120	80	0	260	0
60	120	80	60	260	60
120	120	80	120	260	120
180	120	80	180	260	180
240	120	80	240	260	240
300	120	80	300	260	300
0	180	100	0	280	0
60	180	100	60	280	60
120	180	100	120	280	120
180	180	100	180	280	180
240	180	100	240	280	240
300	180	100	300	280	300
0	240	140	0	320	0
60	240	140	60	320	60
120	240	140	120	320	120
180	240	140	180	320	180
240	240	140	240	320	240
300	240	140	300	320	300
0	300	160	0	340	0
60	300	160	60	340	60
120	300	160	120	340	120
180	300	160	180	340	180
240	300	160	240	340	240
300	300	160	300	340	300

air-ground approach, employing HAPs, provides lower latency as HAPs operate closer to the ground, flexible deployment and repositioning capabilities, and generally lower costs. Despite these advantages, HAPs have smaller coverage areas, are susceptible to weather conditions which can impact their stability and performance, and have shorter operational lifespans requiring more frequent maintenance.

III. METHODOLOGY

In this section, we provide a detailed overview of the methodologies employed in our simulation. Specifically, We describe the channel models that simulate quantum communication links between nodes. Also, we propose an entanglement routing algorithm to facilitate entanglement distribution and performance evaluation. Finally, we upgrade an existing quantum network simulator to conduct our analysis.

A. Channel Models

In this paper, we use fiber optic channels to connect ground nodes, while FSO channels are employed between satellites, and for connecting satellites and the HAP with ground nodes. For each channel, transmissivity is used as a metric to characterize the optical losses encountered during communication. An amplitude damping channel is used to degrade quantum states based on the transmissivity, which is incorporated into the Kraus operator of the amplitude damping channel [16], [17]. Therefore, there is a direct relationship

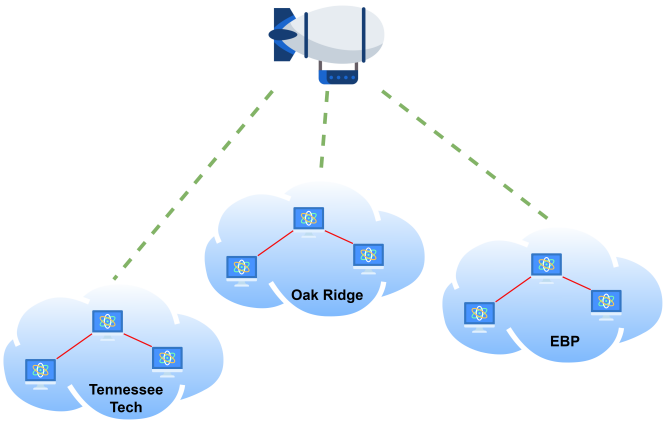

Fig. 4. Illustration of the air-ground architecture employing HAP to connect three local networks in Tennessee. Fiber optic channels are presented in red solid lines, while FSO channels are presented in green dashed lines.

between transmissivity and the fidelity of entanglement states. Consequently, the connections and disconnections between network nodes are governed by a transmissivity threshold that meets the fidelity requirements of specific applications.

1) Fiber Optic Channels: For a transmission distance l and attenuation coefficient α, the fiber optic channel transmissivity is given by [18]

$$\eta = e^{-\alpha l}, \tag{1}$$

2) FSO Channels: The transmissivity of an FSO channel is given by [19]

$$\eta = \eta_{lt}\eta_{atm}\eta_{eff}, \tag{2}$$

where η_{lt}, η_{atm}, and η_{eff} represent the turbulence transmissivity as defined in [Eq. 16, 19], atmospheric loss as defined in [Eq. 19, 19], and receiver efficiency.

3) Amplitude damping channel: The amplitude damping channel is a quantum channel model that represents the reduction or damping of a quantum system's state over time. It characterizes physical processes that lead to the loss of quantum information or the decay of quantum states. In the context of quantum communication, this channel is used to simulate the attenuation of quantum signals during transmission. We use the amplitude damping channel to account for the degradation in entanglement quality based on transmissivity η. This channel can be mathematically described using the Kraus operator as follows [16], [17], [20]

$$\boldsymbol{K_0} = \begin{bmatrix} 1 & 0 \\ 0 & \sqrt{\eta} \end{bmatrix}, \boldsymbol{K_1} = \begin{bmatrix} 0 & \sqrt{1-\eta} \\ 0 & 0 \end{bmatrix}. \tag{3}$$

The effect of the amplitude damping channel on the density matrix $\boldsymbol{\rho}$ is described by

$$\boldsymbol{\rho'} = \boldsymbol{K_0}\boldsymbol{\rho}\boldsymbol{K_0}^\dagger + \boldsymbol{K_1}\boldsymbol{\rho}\boldsymbol{K_1}^\dagger. \tag{4}$$

4) Entanglement Fidelity: Entanglement fidelity, F_e, is used to measure how closely a given entangled state matches the ideal entangled state [21]. In this paper, we employ entanglement fidelity to evaluate the performance of the network architecture based on the quality of the end-to-end entanglement established between the source and destination. The entanglement fidelity is defined by [22] and [21] as follows

$$F_e = \left(\mathrm{Tr}\left(\sqrt{\sqrt{\boldsymbol{\rho'}}\,|\psi\rangle\langle\psi|\,\sqrt{\boldsymbol{\rho'}}}\right)\right)^2, \tag{5}$$

where Tr denotes the trace operator, $\boldsymbol{\rho'}$ denotes the density matrix of the entangled state after undergoing losses, as described by (4), and $|\psi\rangle$ refers to the ideal entangled state. Specifically, $|\psi\rangle$ is the maximally entangled Bell state, represented by $\frac{|00\rangle+|11\rangle}{\sqrt{2}}$.

B. Entanglement Routing

This paper adopts the Bellman-Ford algorithm for entanglement routing based on the transmissivity metric. The selection of transmissivity is driven by its direct impact on the density matrix, as shown in (4), which subsequently impacts the entanglement quality, as reflected in the entanglement fidelity in (5). Originally, Bellman-Ford aimed to minimize the total distance, so the transmissivity metric cannot replace the distance directly because the larger the transmissivity metric, the better. Also, transmissivity is measured between 0 and 1 (i.e., $0 \leq \eta \leq 1$). For this reason, $1/(\eta+\epsilon)$ is used as the cost metric to be minimized, where ϵ is a small positive value that prevents a division by 0. The adopted routing algorithm functions as follows:

1. Each node creates a routing table, setting the cost to reach itself to zero, the cost to reach adjacent nodes to $1/(\eta+\epsilon)$, and the costs to reach all other nodes to ∞.
2. Adjacent nodes exchange their constructed routing tables with each other.
3. Each node updates the cost to reach each node by selecting the minimum cost between directly visiting the node and visiting it through an adjacent node.
4. Steps 2 and 3 are repeated $N-1$ times, where N represents the total number of nodes in the network.

The pseudocode of the routing algorithm is given in Algorithm 1, which defines three main functions BELLMANFORD, INITIALIZE, and UPDATE. The INITIALIZE function performs step 1 for a single node, setting up the initial routing table (R) entries. The UPDATE function performs step 3 for a single node. The BELLMANFORD function calls the two other functions to apply the steps of the algorithm for each node and performs step 4 as well. During the simulation, step 2 is omitted because the simulation is carried out on the same machine and routing tables of other nodes are accessible.

C. Experimental Setup: Quantum Network Simulator

Existing quantum network simulators such as QuNetSim [23], NetSquid [24], QDNS [25], SQUANCH [26], SeQUeNCe [27], SimulaQron [28], and SimQN [29] are primarily limited to ground nodes. To the best of our knowledge, no available simulator can evaluate the performance of proposed quantum network architectures. To address this limitation, we have upgraded the QuNetSim simulator [23] and integrated it with the Ansys Systems Tool Kit (STK) [30]. Although

Algorithm 1 Proposed Quantum Routing Algorithm

```
BellmanFord(Network_Graph)
    for i ∈ G.nodes do
        Initialize(Network_Graph, i)
    end for
    for i from 1 ← Length(G.nodes) − 1 do
        for i ∈ G.nodes do
            Update(Network_Graph, i)
        end for
    end for
Initialize(G, node)
    for i ∈ G.nodes do
        if i = node then
            node.R[i] ← {0, node}
        else if node.isAdjacent(i) then
            node.R[i] ← {1/(η + ϵ), i}
        else
            node.R[i] ← {∞, Null}
        end if
    end for
Update(G, node)
    for (u, v) ∈ G.edges do
        if node.R[u] > node.R[v] + v.R[u] then
            node.R[u] ← {node.R[v]+v.R[u], v}
        end if
    end for
```

QuNetSim supports fiber optic channels, it lacks implementation for FSO channels. Therefore, we introduced an FSO channel as defined in Section III-A2. Specifically, a new class is defined for the FSO channel within the simulator, configuring channel properties via its constructor and calculating transmissivity using (2). Additionally, we extended QuNetSim's *Host* class to include location data such as latitude, longitude, and altitude for ground nodes. New classes are also introduced for satellites and HAPs, inheriting from the *Host* class and incorporating properties specific to each host type. For instance, the *Satellite* class contains a movement list that stores the satellite's sequential locations. A thread is implemented to continuously update the satellite's location, moving it to the next position in the movement list. As the satellite moves, it recalculates the distance to each connected node, leading to updated transmissivity values. Functions are also developed to model the degradation of entangled states and to measure entanglement fidelity as defined in Sections III-A3 and III-A4, respectively. Additionally, the STK simulator is utilized to model satellite movements. Each satellite is initialized in its orbit, and the simulation runs to track satellite movements throughout a day, recording positions at 30-second intervals. These recorded positions generate movement sheets detailing each satellite's precise locations. These movement sheets are then imported into the upgraded QuNetSim. When a satellite node is created, its corresponding movement sheet is mapped and assigned to its movement list.

D. Assumptions Used

Our simulation assumes a perfect setup and ideal conditions, including stable weather, stable flight for HAPs, unlimited flight time, and infinite queue capacity. Specifically, we assume that each node can serve all entanglement requests while in range. This means that whenever the transmissivity threshold is met and a link is established, the nodes can handle all requests for entanglement distribution without limitations. These assumptions are made to generate preliminary results and will be adjusted in future research to better reflect real-world conditions.

IV. Simulation Results and Analysis

Satellites move in their orbits, ground nodes remain stationary, and HAPs hover in place. Links are established between network nodes based on a predefined transmissivity threshold. The connections between ground nodes and HAPs, as well as between ground nodes and other ground nodes, are fixed. Connections and disconnections of satellite links are dynamically updated based on this transmissivity threshold. The attenuation coefficient for fiber optic channels is set to 0.15 dB/km [18]. Simulation parameters for FSO channels follow the configuration outlined in [19], except for the aperture size and the elevation angle. The aperture size for satellites and ground nodes is set to 120 cm [31], while for HAPs, it is set to 30 cm [32], [33]. The elevation angle is set to $\pi/9$.

A. Identifying the Transmissivity Threshold

To determine the transmissivity threshold required for high-fidelity entanglement distribution, we conducted an experiment analyzing the relationship between transmissivity and entanglement fidelity. In this experiment, we established quantum links with transmissivity values ranging from 0 to 1, incremented by 0.01, and measured the resulting fidelity. For simplicity, we used two ground nodes connected by a fiber optic channel, given that the relationship between transmissivity and entanglement fidelity is consistent across various node and channel types, as described in Equation (3) and (4). The results of this analysis are illustrated in Fig. 5. Our findings reveal that a transmissivity of 0.7 yields an entanglement fidelity greater than 90%, which is sufficient for high-fidelity teleportation and quantum information exchange [34], [35]. Consequently, we have set the transmissivity threshold to 0.7. It should be noted that this threshold may be adjusted to meet the specific fidelity requirements of specific applications.

B. Space-Ground Approach

To determine the number of satellites needed to connect the three networks, we analyze the coverage period of the space-ground network. The coverage period is defined as the total duration within an entire day during which all three local networks are interconnected through the satellite constellation. This period may consist of multiple intervals during which connectivity is established. To elaborate, let N_i be a node in a local network i and N_j be a node in a local network j. The coverage period is the total time during which there exists at

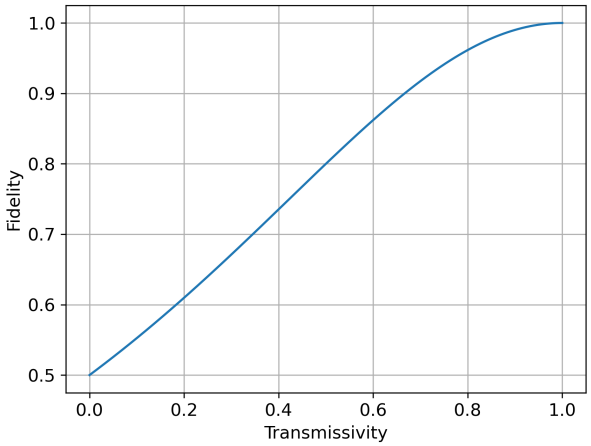

Fig. 5. Relationship between transmissivity and entanglement fidelity.

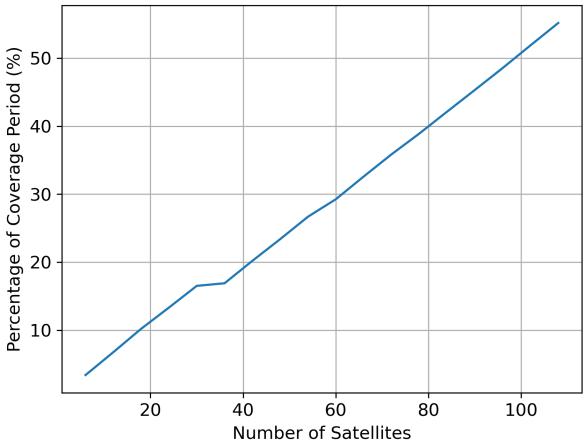

Fig. 6. Coverage percentage of the space-ground network as a function of the number of satellites.

least one satellite link S_{ij} enabling entanglement distribution between every pair of nodes (N_i, N_j), where $i \neq j$, across the three local networks. The coverage period T_c is measured in minutes and calculated as

$$T_c = \sum_k \left(t_{\text{end},k} - t_{\text{start},k}\right), \tag{6}$$

where $t_{\text{start},k}$ and $t_{\text{end},k}$ denote the start and end times of each connected interval k. The percentage of the coverage period P provides a measure of how effectively the satellite constellation maintains connectivity across the networks throughout the day. Herein, P is given by

$$P = \frac{T_c}{T_{\text{day}}} \times 100\%, \tag{7}$$

where T_{day} represents the total duration of the day (1440 minutes). We measure the percentage of the coverage period for a dynamic number of satellites, starting from 6 and increasing incrementally by 6 up to 108 satellites. As shown in Fig. 6, 108 satellites are required to provide coverage for 55.17% of the day.

In Fig. 7, we measure the percentage of served requests between the three local networks. For this experiment, we generate 100 random requests between the three local networks, ensuring that the source and destination are in different local networks. We then record the number of requests that are successfully served and those that remain unserved. This process is repeated over 100 time steps of satellite movement and we report the average performance. Similarly, we experimented with varying numbers of satellites ranging from 6 to 108. As shown in Fig. 7, at least 108 satellites are required to meet 57.75% of entanglement distribution demand.

Finally, we evaluate the entanglement fidelity of the entanglement pairs that can be distributed across the network. For this experiment, we generate 100 random requests between the three local networks, ensuring that the communication parties are in different local networks. For each request, the proposed Bellman-Ford algorithm is used to find the optimal

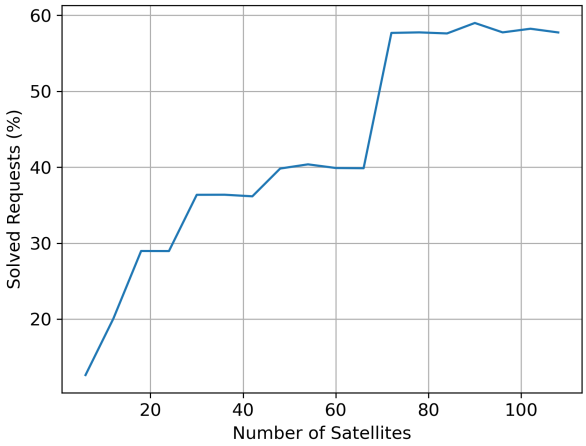

Fig. 7. Served entanglement distribution requests between the three local networks.

path between the source and destination. Subsequently, entanglement pairs are distributed between them and the end-to-end entanglement fidelity is measured and recorded. This process is repeated over 100 time steps of satellite movement. The average entanglement fidelity is then calculated for the resolved requests. The experiment is conducted with a varying number of satellites from 6 to 108. As shown in Fig. 8, the average entanglement fidelity achieved using the space-ground architecture is 0.96.

C. Air-Ground Architecture

Unlike satellites, the HAP hovers in place and is continuously available during its flight time. Therefore, this architecture can provide coverage for the entire day and serve 100% of the entanglement distribution requests. This capability is confirmed by simulations, which demonstrate the performance of the air-ground architecture in maintaining connectivity and fulfilling all entanglement distribution requests. To evaluate

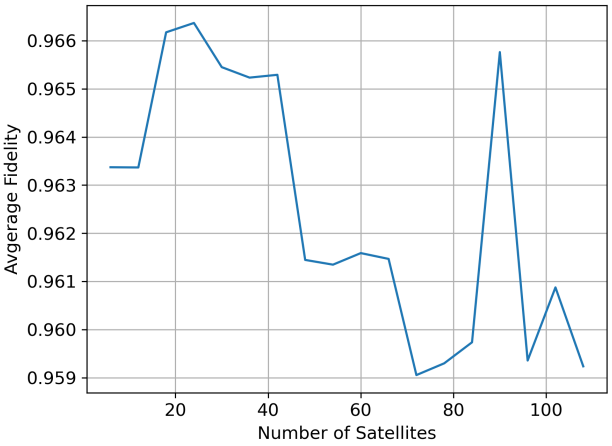

Fig. 8. Average entanglement fidelity for resolved requests between the three local networks.

the performance of this architecture in terms of entanglement fidelity, we generate 100 random entanglement distribution requests between the three networks, ensuring that the source and destination are in different networks. The Bellman-Ford algorithm is then used and entanglement pairs are distributed to the source and destination. Then, the end-to-end entanglement fidelity is measured and recorded. The simulation results show that the air-ground architecture can distribute entanglement pairs with an average entanglement fidelity of 0.98.

D. Comparative Analysis

The space-ground architecture using 108 satellites provides coverage for 55.17% of the day, while the air-ground architecture provides coverage for 100% of the day, effectively enhancing coverage by 44.83%. Additionally, the space-ground architecture can serve 57.75% of entanglement distribution requests, whereas the air-ground architecture can serve 100% of requests, resulting in a 42.25% improvement in the number of resolved entanglement distribution requests. Furthermore, the space-ground architecture achieves an average entanglement fidelity of 0.96, while the air-ground architecture achieves an average fidelity of 0.98, representing a 2% improvement. These enhancements can be attributed to the lower altitude of HAPs, which reduces signal loss and improves fidelity. Additionally, the fixed position of HAPs allows for superior coverage and request handling compared to satellites, whose coverage is limited by their orbits and movement. Table III provides a comparison between the space-ground and air-ground architectures. Despite these advantages, our simulations are carried out under perfect setup and ideal conditions. It is worth mentioning that the air-ground architecture faces significant challenges. One major challenge is the limited flight time of HAPs due to power constraints. Additionally, HAPs are susceptible to environmental factors such as vibrations, which can impact the stability and accuracy of entanglement distribution. Moreover, adverse weather conditions not only degrade signal transmission but also impact the stability of the HAP, posing additional challenges to maintaining consistent and reliable communication links. Addressing these challenges requires further research and the development of advanced technologies to ensure reliable and continuous operation.

TABLE III
SATELLITES ORBITAL CONFIGURATIONS.

Architecture	P	Serving requests	Entanglement fidelity
Space-Ground	55.17%	57.75%	0.96
Air-Ground	100%	100%	0.98

V. CONCLUSION

In this paper, we have explored and compared two approaches for connecting local quantum networks across three cities in Tennessee: a space-ground architecture utilizing satellite constellations and an air-ground architecture employing HAPs. Our findings reveal that the space-ground architecture requires a substantial number of satellites to achieve moderate coverage and request fulfillment, while the air-ground approach offers continuous coverage and higher performance in both serving requests and entanglement fidelity. However, our simulations are carried out under perfect setup and ideal conditions. It is important to note that HAPs have limitations in operational time, coverage area, and susceptibility to environmental factors such as vibrations and weather conditions. Future work should focus on addressing these limitations. Specifically, we will study the impact of environmental factors on HAP stability and signal transmission and develop countermeasures to mitigate the effects of vibrations and adverse weather conditions. By addressing these challenges, we aim to transition from an idealized model to a more realistic and robust implementation, ensuring that quantum networks can be deployed effectively in real-world scenarios. Additionally, we will study how each architecture will deviate from the ideal scenario when considering real-world constraints. Subsequently, we will investigate hybrid solutions that combine the strengths of both space-ground and air-ground architectures. This hybrid approach could potentially mitigate the challenges faced by each architecture and enhance the overall performance and resilience of quantum networks.

REFERENCES

[1] M. Hillery, V. Bužek, and A. Berthiaume, "Quantum secret sharing," *Phys. Rev. A*, vol. 59, pp. 1829–1834, Mar 1999. [Online]. Available: https://link.aps.org/doi/10.1103/PhysRevA.59.1829

[2] G. Brassard, "Quantum communication complexity," *Foundations of Physics*, vol. 33, no. 11, pp. 1593–1616, Nov 2003. [Online]. Available: https://doi.org/10.1023/A:1026009100467

[3] M. Ganz, "Quantum leader election," 2016. [Online]. Available: https://arxiv.org/abs/0910.4952

[4] V. Scarani, H. Bechmann-Pasquinucci, N. J. Cerf, M. Dušek, N. Lütkenhaus, and M. Peev, "The security of practical quantum key distribution," *Reviews of Modern Physics*, vol. 81, no. 3, p. 1301–1350, Sep. 2009. [Online]. Available: http://dx.doi.org/10.1103/RevModPhys.81.1301

[5] J. F. Fitzsimons, "Private quantum computation: an introduction to blind quantum computing and related protocols," *npj Quantum Information*, vol. 3, no. 1, p. 23, Jun 2017. [Online]. Available: https://doi.org/10.1038/s41534-017-0025-3

[6] N. Shettell, M. Hassani, and D. Markham, "Private network parameter estimation with quantum sensors," 2022. [Online]. Available: https://arxiv.org/abs/2207.14450

[7] V. Danos, E. D'Hondt, E. Kashefi, and P. Panangaden, "Distributed measurement-based quantum computation," *Electronic Notes in Theoretical Computer Science*, vol. 170, pp. 73–94, Jun 2005. [Online]. Available: https://doi.org/10.1016/j.entcs.2006.12.012

[8] Y. Huang, F. Salces–Carcoba, R. X. Adhikari, A. H. Safavi-Naeini, and L. Jiang, "Vacuum beam guide for large scale quantum networks," *Physical Review Letters*, vol. 133, no. 2, Jul. 2024. [Online]. Available: http://dx.doi.org/10.1103/PhysRevLett.133.020801

[9] S. C. Williams, "New method could yield fast, cross-country quantum network," *Pritzker School of Molecular Engineering — The University of Chicago.*, Jul. 2024, [Accessed Jul. 2024]. [Online]. Available: https://pme.uchicago.edu/news/new-method-could-yield-fast-cross-country-quantum-network

[10] C.-Y. Lu, Y. Cao, C.-Z. Peng, and J.-W. Pan, "Micius quantum experiments in space," *Rev. Mod. Phys.*, vol. 94, p. 035001, Jul 2022. [Online]. Available: https://link.aps.org/doi/10.1103/RevModPhys.94.035001

[11] "The european quantum communication infrastructure (EuroQCI) initiative." [Online]. Available: https://digital-strategy.ec.europa.eu/en/policies/european-quantum-communication-infrastructure-euroqci

[12] D. Earl, K. Karunaratne, J. Schaake, R. Strum, P. Swingle, and R. Wilson, "Architecture of a first-generation commercial quantum network," 2022. [Online]. Available: https://arxiv.org/abs/2211.14871

[13] E. Bersin, M. Grein, M. Sutula, R. Murphy, Y. Q. Huan, M. Stevens, A. Suleymanzade, C. Lee, R. Riedinger, D. J. Starling, P.-J. Stas, C. M. Knaut, N. Sinclair, D. R. Assumpcao, Y.-C. Wei, E. N. Knall, B. Machielse, D. D. Sukachev, D. S. Levonian, M. K. Bhaskar, M. Lončar, S. Hamilton, M. Lukin, D. Englund, and P. B. Dixon, "Development of a boston-area 50-km fiber quantum network testbed," *Physical Review Applied*, vol. 21, no. 1, Jan. 2024. [Online]. Available: http://dx.doi.org/10.1103/PhysRevApplied.21.014024

[14] D. Ribezzo, M. Zahidy, I. Vagniluca, N. Biagi, S. Francesconi, T. Occhipinti, L. K. Oxenløwe, M. Lončarić, I. Cvitić, M. Stipčević, Pušavec, R. Kaltenbaek, A. Ramšak, F. Cesa, G. Giorgetti, F. Scazza, A. Bassi, P. De Natale, F. Saverio Cataliotti, M. Inguscio, D. Bacco, and A. Zavatta, "Towards a european quantum network," in *2022 European Conference on Optical Communication (ECOC)*, 2022, pp. 1–4.

[15] R. Yehia, M. Schiavon, V. M. Acosta, T. Coopmans, I. Kerenidis, D. Elkouss, and E. Diamanti, "Connecting quantum cities: simulation of a satellite-based quantum network," *New Journal of Physics*, vol. 26, no. 7, p. 073015, jul 2024. [Online]. Available: https://dx.doi.org/10.1088/1367-2630/ad5b13

[16] J. L. Pereira and S. Pirandola, "Bounds on amplitude-damping-channel discrimination," *Phys. Rev. A*, vol. 103, p. 022610, Feb 2021. [Online]. Available: https://link.aps.org/doi/10.1103/PhysRevA.103.022610

[17] A. D'Arrigo, G. Benenti, G. Falci, and C. Macchiavello, "Classical and quantum capacities of a fully correlated amplitude damping channel," *Phys. Rev. A*, vol. 88, p. 042337, Oct 2013. [Online]. Available: https://link.aps.org/doi/10.1103/PhysRevA.88.042337

[18] M. Mobayenjarihani, G. Vardoyan, and D. Towsley, "Optimistic entanglement purification with few quantum memories," in *Proc. of IEEE International Conference on Quantum Computing and Engineering (QCE)*, Broomfield, CO, USA, Oct. 2021, pp. 439–440.

[19] M. Ghalaii and S. Pirandola, "Quantum communications in a moderate-to-strong turbulent space," *Communications Physics*, vol. 5, no. 1, p. 38, Feb 2022. [Online]. Available: https://doi.org/10.1038/s42005-022-00814-5

[20] M. Grassl, L. Kong, Z. Wei, Z.-Q. Yin, and B. Zeng, "Quantum error-correcting codes for qudit amplitude damping," *IEEE Transactions on Information Theory*, vol. 64, no. 6, pp. 4674–4685, 2018.

[21] F. Tonolini, S. Chan, M. Agnew, A. Lindsay, and J. Leach, "Reconstructing high-dimensional two-photon entangled states via compressive sensing," *Scientific Reports*, vol. 4, no. 1, p. 6542, Oct 2014. [Online]. Available: https://doi.org/10.1038/srep06542

[22] R. Jozsa, "Fidelity for mixed quantum states," *Journal of Modern Optics*, vol. 41, no. 12, pp. 2315–2323, 1994. [Online]. Available: https://doi.org/10.1080/09500349414552171

[23] S. Diadamo, J. Nötzel, B. Zanger, and M. M. Beşe, "QuNetSim: A software framework for quantum networks," *IEEE Transactions on Quantum Engineering*, vol. 2, pp. 1–12, 2021.

[24] T. Coopmans, R. Knegjens, A. Dahlberg, D. Maier, L. Nijsten, J. de Oliveira Filho, M. Papendrecht, J. Rabbie, F. Rozpedek, M. Skrzypczyk, L. Wubben, W. de Jong, D. Podareanu, A. Torres-Knoop, D. Elkouss, and S. Wehner, "Netsquid, a network simulator for quantum information using discrete events," *Communications Physics*, vol. 4, no. 1, p. 164, Jul 2021. [Online]. Available: https://doi.org/10.1038/s42005-021-00647-8

[25] O. S. Ceylan and Yılmaz, "QDNS: Quantum dynamic network simulator based on event driving," in *Proc. of International Conference on Information Security and Cryptology (ISCTURKEY)*, Ankara, Turkey, Dec. 2021, pp. 45–50.

[26] B. Bartlett, "A distributed simulation framework for quantum networks and channels," 08 2018.

[27] X. Wu, A. Kolar, J. Chung, D. Jin, T. Zhong, R. Kettimuthu, and M. Suchara, "SeQUeNCe: a customizable discrete-event simulator of quantum networks," *Quantum Science and Technology*, vol. 6, no. 4, p. 045027, Sep. 2021. [Online]. Available: https://dx.doi.org/10.1088/2058-9565/ac22f6

[28] A. Dahlberg and S. Wehner, "SimulaQron—a simulator for developing quantum internet software," *Quantum Science and Technology*, vol. 4, no. 1, p. 015001, Sep. 2018. [Online]. Available: https://dx.doi.org/10.1088/2058-9565/aad56e

[29] L. Chen, K. Xue, J. Li, N. Yu, R. Li, Q. Sun, and J. Lu, "Simqn: A network-layer simulator for the quantum network investigation," *IEEE Network*, vol. 37, no. 5, pp. 182–189, 2023.

[30] AGI, "Ansys STK — digital mission engineering software." [Online]. Available: https://www.ansys.com/products/missions/ansys-stk

[31] H. Li, Y. Huang, Q. Wang, D. He, Z. Peng, and Q. Li, "Performance analysis of satellite-to-ground coherent optical communication system with aperture averaging," *Applied Sciences*, vol. 8, no. 12, 2018. [Online]. Available: https://www.mdpi.com/2076-3417/8/12/2496

[32] T. Okura, H. Tsuji, R. Miura, T. Kan, T. Matsuda, M. Toyoshima, J. Suzuki, and Y. Kishiyama, "Prototype evaluation of the 38ghz-band lens antenna for high altitude platform station (haps) ground station system," in *2021 24th International Symposium on Wireless Personal Multimedia Communications (WPMC)*, 2021, pp. 1–5.

[33] N. Perlot, E. Duca, J. Horwath, D. Giggenbach, and E. Leitgeb, "System requirements for optical hap-satellite links," in *2008 6th International Symposium on Communication Systems, Networks and Digital Signal Processing*, 2008, pp. 72–76.

[34] D. Nield, "Quantum teleportation was just achieved with 90% accuracy over a 44km distance," Dec 2020. [Online]. Available: https://www.sciencealert.com/scientists-achieve-sustained-high-fidelity-quantum-teleportation-over-44-km

[35] R. Valivarthi, S. I. Davis, C. Peña, S. Xie, N. Lauk, L. Narváez, J. P. Allmaras, A. D. Beyer, Y. Gim, M. Hussein, G. Iskander, H. L. Kim, B. Korzh, A. Mueller, M. Rominsky, M. Shaw, D. Tang, E. E. Wollman, C. Simon, P. Spentzouris, D. Oblak, N. Sinclair, and M. Spiropulu, "Teleportation systems toward a quantum internet," *PRX Quantum*, vol. 1, p. 020317, Dec 2020. [Online]. Available: https://link.aps.org/doi/10.1103/PRXQuantum.1.020317